






Article

Radiative Cascade Repopulation of $1s2s2p\ ^4P$ States Formed by Single Electron Capture in 2–18 MeV Collisions of $C^{4+} (1s2s\ ^3S)$ with He

Theo J. M. Zouros ^{1,2,*} , Sofoklis Nikolaou ^{3,4}, Ioannis Madesis ^{1,2} , Angelos Laoutaris ^{1,2} , Stefanos Nanos ^{2,5} , Alain Dubois ⁶ and Emmanouil P. Benis ⁵ 

¹ Department of Physics, University of Crete, GR-70013 Heraklion, Greece; imadesis@physics.uoc.gr (I.M.); laoutaris@physics.uoc.gr (A.L.)

² Tandem Accelerator Laboratory, Institute of Nuclear and Particle Physics, NCSR “Demokritos”, GR-15310 Agia Paraskevi, Greece; nanos@inp.demokritos.gr

³ Department of Electronic Engineering, Hellenic Mediterranean University, GR-73133 Chania, Greece; sofnik21@gmail.com

⁴ Institute of Plasma Physics & Lasers, Hellenic Mediterranean University, GR-74100 Tria Monastiria, Rethymno, Greece

⁵ Department of Physics, University of Ioannina, GR-45110 Ioannina, Greece; mbenis@uoi.gr

⁶ Laboratoire de Chimie Physique-Matière et Rayonnement, Sorbonne Université, CNRS, F-75005 Paris, France; alain.dubois@sorbonne-universite.fr

* Correspondence: tzouros@physics.uoc.gr

Received: 7 August 2020; Accepted: 12 September 2020; Published: 21 September 2020



Abstract: This study focuses on the details of cascade repopulation of doubly excited triply open-shell $C^{3+} (1s2s2p)\ ^4P$ and $^2P_{\pm}$ states produced in 2–18 MeV collisions of $C^{4+} (1s2s\ ^3S)$ with He. Such cascade calculations are necessary for the correct determination of the ratio R of their cross sections, used as a measure of spin statistics [Madesis et al. PRL **124** (2020) 113401]. Here, we present the details of our cascade calculations within a new matrix formulation based on the well-known diagrammatic cascade approach [Curtis, Am. J. Phys. **36** (1968) 1123], extended to also include Auger depopulation. The initial populations of the $1s2snl\ ^4L$ and $1s2snl\ ^2L$ levels included in our analysis are obtained from the direct $n\ell$ single electron capture (SEC) cross sections, calculated using the novel three-electron close-coupling (3eAOCC) approach. All relevant radiative branching ratios (RBR) for $n \leq 4$ were computed using the COWAN code. While doublet RBRs are found to be very small, quartet RBRs are found to be large, indicating cascade feeding to be important only for quartets, consistent with previous findings. Calculations including up to third order cascades, extended to $n \rightarrow \infty$ using an n^{-3} SEC model, showed a $\sim 60\%$ increase of the $1s2s2p\ ^4P$ populations due to cascades, resulting, for the first time, in R values in good overall agreement with experiment.

Keywords: cascade feeding; single electron capture; cascade matrix; mixed-state beams; metastable states; Li-like states; He-like states; zero-degree Auger projectile spectroscopy; 3eAOCC

1. Introduction

Highly excited (autoionizing) atomic and ionic states can be produced in ion-atom and ion-electron collisions by various processes such as inner-shell excitation, ionization, electron capture (to excited states), and/or their combinations. These states then relax to lower energy states and the ground state via radiative and/or Auger decays in a stepwise manner, known as cascades, resulting in the repopulation of the intermediate levels. Cascade repopulation of intermediate levels is also common to atoms and multi-charged ions in laboratory plasmas [1,2], as well as astrophysical plasmas encountered

in solar coronas, gas nebulae and active galactic nuclei (AGN) [1,3,4]. The complex character of the stepwise cascade process, an inherent, but usually unwanted side effect in most investigations, has received considerable attention, studied primarily by simulations [5–8]. Such studies have focused on mostly radiative cascades related to recombination in He-like ions [9], emission of polarized X-rays [10], X-ray fusion diagnostics [11], shake-off effects [12], solar wind [13] and electron capture in H-like ions [14–16], just to mention a few. Cascade repopulation affects the accurate determination of cross sections, therefore adding uncertainty in the comparison with theory, which eventually must also include the additional cascade contributions by performing a detailed cascade feeding analysis. Moreover, cascades have been an ever present limitation in the precise determination of lifetimes [17] using beam-foil spectroscopy [18–22].

Some of the most investigated states in ion-atom collisions are the Li-like doubly excited quartet $1s2snl\ ^4L$ states. In particular, the lowest-lying $1s2s2p\ ^4P$ state, which is also metastable, has been under study since the early 70s, first observed in the ions of Be^+ , B^{2+} and F^{6+} [23], C^{3+} [24], O^{5+} and F^{6+} [25,26], Li [27], as well as in highly charged heavier ions such as Cl^{14+} and Ar^{15+} [28]. For a general review of optical studies of these states, see also [29] and references therein.

Of more recent interest has been the ratio R of $1s2s2p\ ^4P/{}^2P$ cross sections [30]. In the case of $2p$ single electron capture (SEC) in collisions of $1s2s\ ^3S$ ions with He and H_2 , R has been considered to be an indicator of spin statistics [31–35]. Indeed, this ratio results in $R = 1$, when considering only spin multiplicity, while $R = 2$ in the frozen core approximation, where only the 4P and a single 2P state can be produced from the $1s2s\ ^3S$ initial state [34,36,37]. Such statistical arguments and approximations are often used to simplify difficult problems of computing relative populations in high energy plasmas [4] and can therefore be of important practical use. Very recently, we reported [30] that in collisions using C^{4+} ($1s2s\ ^3S$) projectile ions, a complete breakdown of the frozen core treatment used for SEC to date is observed, as regards to spin statistics in this highly correlated dynamical atomic system. Furthermore, we showed that only a new dynamical calculation involving three active electrons is found to give results consistent with experiment, with radiative cascade repopulation playing an important role.

Here, we present the details of modeling this radiative cascade feeding of the doubly excited C^{3+} $1s2s2p\ ^4P$ and $1s2s2p\ ^2P$ levels formed by SEC. Our cascade calculation is based on a new, elegant, and easy to use matrix formulation extending the well-known diagrammatic approach of Curtis [38]. The necessary radiative and Auger transition rates were computed using the COWAN [39] atomic structure code, while the initial state populations were taken from our recent publication [30], where they were computed using the new three-electron atomic orbital close-coupling (3eAOCC) approach.

2. Mathematical Description of Radiative Cascade Feeding

In this section, we present our mathematical description of radiative cascades extending the treatment of Curtis [38] to also include Auger depopulation. These Auger transitions are important in the case of the C^{3+} ($1s2s2p\ ^4,2P$) states [35], to which we apply our otherwise general treatment. An elegant, cascade matrix formulation is used making the cascade calculations much easier to evaluate to any desired cascade order, as required.

2.1. Definitions—The Cascade Rate Equation

We consider a set of m levels labeled consecutively in order of decreasing binding energies E_i from 1 to m . The population at time t of the j -th level denoted $N_j(t)$ with energy E_j is assumed to be the result of cascade feeding from higher energy levels ($k > j$) by radiative transitions with rates A_{kj}^r and photon energies $\hbar\omega_{kj} = E_k - E_j$, as well as depopulation by radiative transitions to all lower energy levels $f = 1, 2, \dots, j-1$, with rates A_{jf}^r . Additional depopulation can also occur due to autoionizing (including Auger and Coster-Kronig) transitions, which remove population from the level j to all final states f' , with the rate $A_{jf'}^a$. The final states f' of the autoionizing transitions correspond to a different set of electronic configurations from those of the radiative transitions (the ion charge is reduced by

one in the case of autoionization) and are therefore denoted by a prime. An example of the schematic decay of a 5-level system ($m = 5$) is shown in Figure 1.

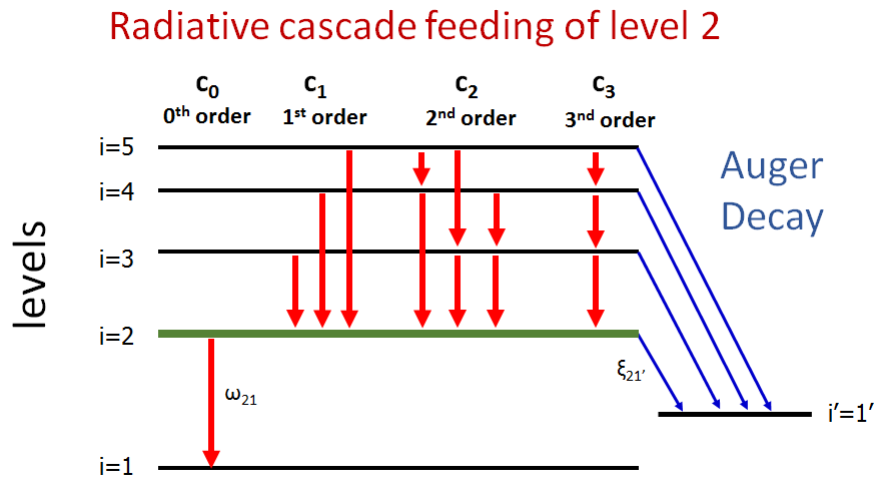


Figure 1. Schematic decay of a 5-level system indicating radiative cascade feeding to the level 2 of interest (i.e., $n = 2$ and $m = 5$ in Equation (1)). The radiative transitions are indicated by red arrows, while Auger transitions by blue arrows. Cascades are separated into feeding orders $c_0, c_1, c_2, c_3, \dots$ requiring, in this example, a total of 0, 1, 2 or 3 sequential transitions, respectively, to reach the chosen level of interest, $i = 2$. Thus, the k -th cascade order c_k results in the emission of k photons along each of the allowed cascade sequences. For simplicity, only one radiative ($f = 1$) and one Auger ($f' = 1'$) final levels are shown. The radiative branching ratios, also known as partial fluorescence yields, are given in general by ω_{ij} (only ω_{21} is shown) for transitions from initial level i to final levels j (see Equation (4)). Also indicated is the partial Auger yield $\xi_{21'}$.

The coupled differential equations governing the population of any particular level $n \in [1, m]$ (i.e., the general index j now has the specific value $j = n$) are then readily given [38] with the addition of the *depopulating* autoionization channel [35]¹ by:

$$\frac{dN_n}{dt} = \sum_{i=n+1}^m A_{in}^r N_i(t) - \left(\sum_{f=1}^{n-1} A_{nf}^r + \sum_{f'} A_{nf'}^a \right) N_n(t) = \sum_{i=n+1}^m A_{in}^r N_i(t) - \alpha_n N_n(t), \quad (1)$$

with α_n defined as²:

$$\alpha_n \equiv \sum_{f=1}^{n-1} A_{nf}^r + \sum_{f'} A_{nf'}^a = \frac{1}{\tau_n}. \quad (2)$$

Thus, α_n is seen to be the *total* decay rate ($= \hbar \Gamma_n$, where Γ_n is the total width) of level n , i.e., the inverse of its lifetime τ_n , and is defined as the sum of *all* transition probabilities between level n and all lower-lying levels, including Auger decays. In α_n (Equation (2)), we now include

¹ It is assumed that any *populating* channel due to autoionization is negligible—this is justified for the system studied here, i.e., energetic collisions of $C^{4+}(1s2s^3S) + He$. In principle, such an autoionizing feeding channel would require the production of Be-like states of the type $C^{2+}(1s2snl'n'l')$ by low probability double capture events, which could then autoionize to the $C^{3+}(1s2snl)$ states considered here and in Ref. [35]. This is not known to happen, but could happen due to Coster-Kronig transitions for other carbon transitions such as $C^{2+}(1s^22pn'l) \rightarrow C^{3+}(1s^22s) + e^-$ for $n \geq 4$ [40] or $C^{3+}(1s2pn'l) \rightarrow C^{4+}(1s2l') + e^-$ for $n \geq 7$ [41].

² The transition rates A_{ij} are related to the corresponding widths $\Gamma_{ij} = \hbar A_{ij}$. It is important not to confuse the *decay* line width $\Gamma(i, j)$, which is the sum of the widths of both initial and final states, $\Gamma(i, j) = \Gamma_i + \Gamma_j$, with the *natural* width of a level Γ_i which is related to its lifetime through the uncertainty relationship, $\tau_i \Gamma_i = \hbar$ or $\Gamma_i = \hbar \alpha_i$.

both radiative and Auger decays, thus extending the treatment of Curtis [38] (which only included the radiative term A_{nf}^r in α_n). This is seen not to change the overall mathematical form of the rate equation which remains:

$$\frac{dN_n}{dt} + \alpha_n N_n(t) = \sum_{i=n+1}^m A_{in}^r N_i(t). \tag{3}$$

It is helpful to also introduce the notions of the *partial* fluorescence yield ω_{nf} and the *partial* Auger yield $\zeta_{nf'}$, in addition to the fluorescence yield ω_n and the Auger yield ζ_n [42]:

$$\omega_{nf} = \frac{A_{nf}^r}{\alpha_n} \quad \text{and} \quad \omega_n = \frac{A_n^r}{\alpha_n}, \tag{4}$$

$$\zeta_{nf'} = \frac{A_{nf'}^a}{\alpha_n} \quad \text{and} \quad \zeta_n = \frac{A_n^a}{\alpha_n}, \tag{5}$$

where we have also introduced the *total* radiative A_n^r and total Auger A_n^a rates for level n :

$$A_n^r \equiv \sum_{f=1}^{n-1} A_{nf}^r \quad \text{and} \quad A_n^a \equiv \sum_{f'} A_{nf'}^a, \tag{6}$$

and therefore we also have:

$$\alpha_n = A_n^r + A_n^a \quad \text{and} \quad \omega_n + \zeta_n = 1. \tag{7}$$

Thus, ω_{nf} and $\zeta_{nf'}$, are equivalent to probabilities for the state n to decay either radiatively or by autoionization to any one of the final states f or f' , respectively. The partial fluorescence yield ω_{ij} is also known as the radiative branching ratio (RBR).

Equation (3) can be readily solved by multiplying both sides by the integrating factor $\exp(\alpha_n t)$ and performing the integration after exchanging the order of sum and integral [38] to give an iterative solution that can be readily programmed to give analytic results:

$$N_n(t) = \left[N_n(0) + \sum_{i=n+1}^m A_{in}^r \int_0^t dt' \exp(\alpha_n t') N_i(t') \right] \exp(-\alpha_n t). \tag{8}$$

Inclusion of the depopulating Auger transitions in the definition of α_n (Equation (2)) does not change the form of the differential equation (Equation (3)), thus having exactly the same solution as Equation (8), like the ones given by Curtis [38]. However, the result is more general and, as seen in the case of the $C^{3+}(1s2s2p\ 4,2P)$ level populations, plays an important role in the detailed understanding of the cascade feeding mechanism, which is found to selectively enhance the population of the quartets compared to that of the doublets [30,33,35].

2.2. Time-Dependence of Level Populations and Cascade Feeding Orders

The first three iterations of Equation (8) can be readily computed after performing the trivial integrations. Defining the radiative cascade feeding orders c_0, c_1, c_2 , we have [38]:

$$c_0 : N_n^{c_0}(t) = N_n(0) \exp(-\alpha_n t), \tag{9}$$

$$\begin{aligned} c_1 : N_n^{c_1}(t) &= \left[\sum_{i=n+1}^m N_i(0) A_{in}^r \int_0^t dt' \exp[(\alpha_n - \alpha_i)t'] \right] \exp(-\alpha_n t) \\ &= \sum_{i=n+1}^m N_i(0) A_{in}^r \left[\frac{\exp(-\alpha_i t)}{(\alpha_n - \alpha_i)} + \frac{\exp(-\alpha_n t)}{(\alpha_i - \alpha_n)} \right], \end{aligned} \tag{10}$$

$$\begin{aligned} c_2 : N_n^{c_2}(t) &= \left[\sum_{i=n+1}^{m-1} \sum_{j=i+1}^m N_j(0) A_{ji}^r A_{in}^r \int_0^t dt' \exp[(\alpha_n - \alpha_i)t'] \int_0^{t'} dt'' \exp[(\alpha_i - \alpha_j)t''] \right] \exp(-\alpha_n t) \\ &= \sum_{i=n+1}^{m-1} \sum_{j=i+1}^m N_j(0) A_{ji}^r A_{in}^r \left[\frac{\exp(-\alpha_j t)}{(\alpha_i - \alpha_j)(\alpha_n - \alpha_j)} + \frac{\exp(-\alpha_i t)}{(\alpha_j - \alpha_i)(\alpha_n - \alpha_i)} + \frac{\exp(-\alpha_n t)}{(\alpha_j - \alpha_n)(\alpha_i - \alpha_n)} \right], \end{aligned} \tag{11}$$

with the total contribution up to and including cascade order c_k , $N_n(t) [\leq c_k]$, readily computed using Equation (8) and given by the sum:

$$N_n(t) [\leq c_k] = N_n^{c_0}(t) + N_n^{c_1}(t) + N_n^{c_2}(t) + \dots + N_n^{c_k}(t) = \sum_{i=0}^k N_n^{c_i}(t). \tag{12}$$

We note that the $t = 0$ initial level populations $N_i(0)$ above, refer to the i -th level populations before cascading begins and are independently calculated, as discussed in detail in Section 3.3.

Referring to Figure 1, the 0-th order cascade term c_0 corresponds to the *depopulating* of level n of interest, either by an Auger or a radiative transition, to all available levels below it, while cascade orders c_k (with $k \geq 1$) correspond to the *populating* of level n from all higher-lying energy levels. The initial population of level n at time $t = 0$, i.e., in the absence of cascade feeding, is usually the *primary* process under investigation. Here, this is the direct $2p$ SEC leading to the production of the $1s2s2p \ 4P$ and $2P$ states detected by their Auger decay [30,43]. The higher order cascades usually constitute an unwanted complication that needs to be understood and quantified before accurate cross section information can be extracted about the population of level n due to just the primary process.

The first-order cascade term c_1 corresponds to the radiative feeding of the level n from all levels i above it, i.e., $n + 1 \leq i \leq m$, by direct *one-step* radiative $\{i \rightarrow n\}$ transitions, i.e., with the emission of 1 photon. The second-order c_2 corresponds to the feeding of the level n from all levels j above it, in a *two-step* radiative transition sequence $\{j \rightarrow i \rightarrow n\}$, with the first step described by the index j with $i + 1 \leq j \leq m$, and the second step by the index i , with the second-step index i within the range $n + 1 \leq i \leq m - 1$. The second step has its upper limit reduced by 1, i.e., $m - 1$, to accommodate the first step which would start in this case from $j = m$, (i.e., $\{j = m \rightarrow i \rightarrow n\}$). Thus, in the c_2 sequence 2 photons are emitted. Similarly, the c_k order results in a sequence of k -steps with the emission of k photons. The contribution of any order k corresponds to the total probability of emitting k sequential photons, each transition contributing with its RBR ω_{ij} , and thus is roughly proportional to the product $(\omega_{ij})^k$, which therefore rapidly decreases with increasing value of k . The maximum permitted order is clearly determined by the number of levels between n and the highest level $m = M$, where M is the maximum number of levels included in the calculation.

In a typical cascade calculation, it is rare to include contributions beyond the 3rd order (c_3), since the convergence of the summation series (Equation (12)) is usually quite rapidly attained. Here, in our calculations (see next sections), we include up to 3rd order cascades, clearly showing that convergence has effectively been attained by c_2 for all, but the lowest collision energies³.

³ At collision energies below 0.3 MeV/u, even higher order cascades might need to be considered since the value of n at which SEC is maximized moves from $n_{max} = 2$ for MeV/u collisions to higher values $n_{max} \sim 3-5$ for keV/u collisions [44].

2.3. Final Level Populations

Integrating the time-dependent population number $N_n(t)$ over a sufficiently long detection time τ_d , so as to include *all* the decaying radiative transitions of interest (dipole E1 transitions typically occur within the lifetime of any level i , i.e., $\tau_i = 1/\alpha_i$, so we need $\alpha_i\tau_d \gg 1$), results in integrals of the type:

$$\int_0^{\tau_d} \exp(-\alpha_i t) dt = \frac{1 - \exp(-\alpha_i \tau_d)}{\alpha_i} \approx \frac{1}{\alpha_i} \quad (\text{for all } \alpha_i \tau_d \gg 1), \tag{13}$$

effectively equivalent to integrating over all time, i.e., $\tau_d \rightarrow \infty$. Thus, integrating over all time, the general expressions for $N_n(t)$ from Equations (9)–(11) for c_0, c_1 and c_2 cascades we have:

$$c_0 : I_n^{c_0} \equiv \int_{t=0}^{\infty} dt N_n^{c_0}(t) = \frac{N_n(0)}{\alpha_n}, \tag{14}$$

$$\begin{aligned} c_1 : I_n^{c_1} &\equiv \int_{t=0}^{\infty} dt N_n^{c_1}(t) = \sum_{i=n+1}^m N_i(0) A_{in}^r \left[\frac{1}{(\alpha_n - \alpha_i)\alpha_i} + \frac{1}{(\alpha_i - \alpha_n)\alpha_n} \right] \\ &= \sum_{i=n+1}^m \frac{N_i(0)}{\alpha_n} \frac{A_{in}^r}{\alpha_i} = \frac{1}{\alpha_n} \sum_{i=n+1}^m N_i(0) \omega_{in}, \end{aligned} \tag{15}$$

$$\begin{aligned} c_2 : I_n^{c_2} &\equiv \int_{t=0}^{\infty} dt N_n^{c_2}(t) \\ &= \sum_{i=n+1}^{m-1} \sum_{j=i+1}^m N_j(0) A_{ji}^r A_{in}^r \left[\frac{1}{\alpha_j(\alpha_i - \alpha_j)(\alpha_n - \alpha_j)} + \frac{1}{\alpha_i(\alpha_j - \alpha_i)(\alpha_n - \alpha_i)} + \frac{1}{\alpha_n(\alpha_j - \alpha_n)(\alpha_i - \alpha_n)} \right] \\ &= \sum_{i=n+1}^{m-1} \sum_{j=i+1}^m \frac{N_j(0)}{\alpha_n} \frac{A_{ji}^r}{\alpha_j} \frac{A_{in}^r}{\alpha_i} = \frac{1}{\alpha_n} \sum_{i=n+1}^{m-1} \sum_{j=i+1}^m N_j(0) \omega_{ji} \omega_{in}, \end{aligned} \tag{16}$$

and similarly for c_3 and so on with

$$c_3 : I_n^{c_3} \equiv \int_{t=0}^{\infty} dt N_n^{c_3}(t) = \frac{1}{\alpha_n} \sum_{l=n+1}^{m-2} \sum_{i=l+1}^{m-1} \sum_{j=i+1}^m N_j(0) \omega_{ji} \omega_{il} \omega_{ln}. \tag{17}$$

This can be readily extended to include cascades to any order c_k so that in general we have:

$$I_n [\leq c_k] = \int_{t=0}^{\infty} dt N_n(t) [\leq c_k] = I_n^{c_0} + I_n^{c_1} + I_n^{c_2} + \dots + I_n^{c_k} = \frac{N_n[\leq c_k]}{\alpha_n} = \sum_{i=0}^k I_n^{c_i},$$

with the total population of level n up to and including order c_k given by:

$$\begin{aligned} N_n [\leq c_k] &\equiv N_n^{c_0} + N_n^{c_1} + N_n^{c_2} + N_n^{c_3} + \dots + N_n^{c_k} = \sum_{i=0}^k N_n^{c_i} \\ &= N_n(0) + \sum_{i=n+1}^m N_i(0) \omega_{in} + \sum_{i=n+1}^{m-1} \sum_{j=i+1}^m N_j(0) \omega_{ji} \omega_{in} + \sum_{l=n+1}^{m-2} \sum_{i=l+1}^{m-1} \sum_{j=i+1}^m N_j(0) \omega_{ji} \omega_{il} \omega_{ln} + \dots, \end{aligned} \tag{18}$$

with:

$$N_n^{c_k} \equiv \alpha_n I_n^{c_k}. \tag{19}$$

These results are clearly what one would intuitively expect by inspecting Figure 1. Thus, in Equation (18), the 0-th cascade order c_0 refers to just the initial occupation number $N_n(t = 0)$. The 1st cascade order, c_1 , requires a *single* radiative transition to feed the state n from all higher-lying states j with probability ω_{jn} and initial occupation number $N_j(0)$, readily given by $\sum_{j=n+1}^m N_j(0) \omega_{jn}$. The 2nd cascade order, c_2 , requires the contributions of all possible two-step radiative transition

pathways ending on level n , i.e., all two-step pathways $\{j \rightarrow i \rightarrow n\}$, with probability ω_{ji} and ω_{in} and starting from all initial states j with occupation number $N_j(0)$. This is readily given by $\sum_{i=n+1}^{m-1} \sum_{j=i+1}^m N_j(0) \omega_{ji} \omega_{in}$, and so on. Thus, the general result for any order can be readily written down simply by inspection of the cascade level diagram. The clarity of this diagrammatic approach is nicely presented by Curtis [38] and summarized here.

2.4. X-ray and Auger Electron Emission Rates

Experimental information about the n level population comes mostly from either X-ray or Auger electron measurements. The rate of X-rays (or Auger electrons) emitted in a transition from the level n to level f (or f' , respectively) is given (in #/s) by [33,45]:

$$\dot{N}_{nf}^x(t) \equiv \frac{dN_{nf}^x}{dt} = N_n(t) A_{nf}^r \quad \text{(characteristic x-rays),} \quad (20)$$

$$\dot{N}_{nf'}^e(t) \equiv \frac{dN_{nf'}^e}{dt} = N_n(t) A_{nf'}^a \quad \text{(Auger electrons).} \quad (21)$$

Noting from Equation (4) that $\omega_{nf} = \frac{A_{nf}^r}{\alpha_n}$ and from Equation (5) that $\zeta_{nf'} = \frac{A_{nf'}^a}{\alpha_n}$, the total number of X-rays or Auger electrons emitted up to and including order c_k is then given by:

$$N_{nf}^x[\leq c_k] = \int_{t=0}^{\infty} dt \dot{N}_{nf}^x(t) = A_{nf}^r I_n[\leq c_k] = \omega_{nf} N_n[\leq c_k] \quad \text{(characteristic x-rays),} \quad (22)$$

$$N_{nf'}^e[\leq c_k] = \int_{t=0}^{\infty} dt \dot{N}_{nf'}^e(t) = A_{nf'}^a I_n[\leq c_k] = \zeta_{nf'} N_n[\leq c_k] \quad \text{(Auger electrons),} \quad (23)$$

with $N_n[\leq c_k]$ given by Equation (18).

Here, we have used the technique of zero-degree Auger projectile spectroscopy (ZAPS) [46] to obtain the level populations of the $1s2s2p^4P$ and $2P_{\pm}$ states [30,43].

2.5. The Cascade Matrix Formulation

The above results can be put into a very practical and general matrix format for any level n of primary interest ($1 \leq n \leq M$) by introducing the upper triangular $M \times M$ matrix $\tilde{\Omega}$ as follows:

$$\tilde{\Omega} = \tilde{\omega}_{ij} = \begin{cases} 0 & j \leq i \\ \omega_{ji} & j > i \end{cases} \quad \text{(where } i = 1, 2, 3, \dots, M \text{ and } j = 1, 2, 3, \dots, M), \quad (24)$$

i.e., $\tilde{\Omega}$ has all its diagonal elements and its lower off-diagonal elements equal to 0 (see example in Equation (27)). The upper off-diagonal elements are the RBRs ω_{ji} , i.e., the partial fluorescence yields for the radiative transition $\{j \rightarrow i\}$. Unfortunately, for array element $\tilde{\omega}_{ij}$, to have its indices in the right order for matrix multiplication, one must have them reversed from the existing notation of ω_{ij} , i.e., $\tilde{\omega}_{ij} = \omega_{ji}$, where j and i are the initial and final level numbers of the transition $\{j \rightarrow i\}$.

With this definition, it can be readily seen from Equation (15) that for any level of interest n in a system of M levels we can write for c_1 :

$$N_n^{c_1} = \alpha_n I_n^{c_1} = \sum_{i=n+1}^M \omega_{in} N_i(0) = \sum_{i=1}^M \tilde{\omega}_{ni} N_i(0), \quad (25)$$

since all elements of $\tilde{\omega}_{ni} = 0$ for $n \leq i$. The last summation in Equation (25) is just the multiplication of the matrix $\tilde{\Omega}$ with column vector N^{c_0} :

$$N^{c_1} = \tilde{\Omega} \otimes N^{c_0}(E_p), \quad (26)$$

where N^{c_0} is the column vector with elements $N_i^{c_0} \equiv (N^{c_0})_i = N_i(0)$, i.e., the population numbers of all $i = 1 \dots M$ levels at time $t = 0$ for the collision energy E_p explicitly noted. Then, in full matrix form (with the n -th entry of interest in bold) this reads:

$$\begin{pmatrix} N_1^{c_1} \\ N_2^{c_1} \\ \dots \\ N_{n-1}^{c_1} \\ \mathbf{N}_n^{c_1} \\ N_{n+1}^{c_1} \\ \dots \\ N_{M-1}^{c_1} \\ N_M^{c_1} \end{pmatrix} = \begin{pmatrix} 0 & \tilde{\omega}_{12} & \tilde{\omega}_{13} & \dots & \dots & \dots & \dots & \dots & \dots & \tilde{\omega}_{1M} \\ 0 & 0 & \tilde{\omega}_{23} & \tilde{\omega}_{24} & \dots & \dots & \dots & \dots & \dots & \tilde{\omega}_{2M} \\ 0 & \dots & 0 & \dots & \dots & \dots & \dots & \dots & \dots & \dots \\ 0 & \dots & \dots & 0 & \tilde{\omega}_{n-1n} & \dots & \dots & \dots & \dots & \tilde{\omega}_{n-1M} \\ \mathbf{0} & \dots & \dots & \dots & \mathbf{0} & \tilde{\omega}_{nn+1} & \dots & \dots & \dots & \tilde{\omega}_{nM} \\ 0 & \dots & \dots & \dots & \dots & 0 & \tilde{\omega}_{n+1n+2} & \dots & \dots & \tilde{\omega}_{n+1M} \\ 0 & \dots & \dots & \dots & \dots & \dots & 0 & \dots & \dots & \dots \\ 0 & \dots & \dots & \dots & \dots & \dots & \dots & 0 & \dots & \tilde{\omega}_{M-1M} \\ 0 & 0 & 0 & 0 & 0 & 0 & 0 & \dots & 0 & 0 \end{pmatrix} \begin{pmatrix} N_1^{c_0} \\ N_2^{c_0} \\ \dots \\ N_{n-1}^{c_0} \\ N_n^{c_0} \\ N_{n+1}^{c_0} \\ \dots \\ N_{M-1}^{c_0} \\ N_M^{c_0} \end{pmatrix}, \tag{27}$$

setting everywhere $\tilde{\omega}_{ij} = \omega_{ji}$, we obtain the c_1 contributions for any level n with $1 \leq n \leq M$.

The second cascade order contributions (c_2) can also be obtained in exactly the same way from the first order (c_1). In fact, from Equation (16) we have:

$$N_n^{c_2} = \alpha_n I_n^{c_2} = \sum_{i=n+1}^{m-1} \sum_{j=i+1}^m \omega_{in} \omega_{ji} N_j(0) = \sum_{i=1}^M \tilde{\omega}_{ni} \sum_{j=1}^M \tilde{\omega}_{ij} N_j(0) = \sum_{i=1}^M \tilde{\omega}_{ni} N_i^{c_1}. \tag{28}$$

Thus, the general formula for cascades of order k (c_k) is seen to be obtained from the immediately lower order $k - 1$ (c_{k-1}) by the following simple algorithm:

$$N_n^{c_k} = \sum_{i=1}^M \tilde{\omega}_{ni} N_i^{c_{k-1}}, \tag{29}$$

or in matrix form:

$$N^{c_k} = \tilde{\Omega} \otimes N^{c_{k-1}} = \tilde{\Omega}^k \otimes N^{c_0}(E_p), \tag{30}$$

where $\tilde{\Omega}^k$ refers to the matrix product of k $\tilde{\Omega}$ matrices. Thus, the total population up to and including contributions of order c_k can be written in column form as:

$$N[\leq c_k] = \sum_{i=0}^k N^{c_i} = \left(\tilde{\Omega}^0 + \tilde{\Omega} + \tilde{\Omega}^2 + \dots + \tilde{\Omega}^k \right) \otimes N^{c_0}(E_p), \tag{31}$$

where $\tilde{\Omega}^0 \equiv I$, is the identity matrix.

We note that the initial population number $N_i(0)$ of each level i is proportional to its (direct) production cross section $\sigma_i (= \sigma_i^{c_0})$:

$$N_i(0) = N_i^{c_0}(0)(E_p) = \kappa \sigma_i^{c_0}(E_p), \tag{32}$$

where the proportionality constant κ depends quite generally only on the particular features of the specific experimental setup. Thus, we may define the cross section column vector S^{c_0} analogous to the population column vector N^{c_0} :

$$N^{c_0}(E_p) = \kappa S^{c_0}(E_p), \tag{33}$$

and then write in analogy with Equation (30):

$$S^{c_k} = \tilde{\Omega} \otimes S^{c_{k-1}} = \tilde{\Omega}^k \otimes S^{c_0}(E_p). \tag{34}$$

Thus, the total cross sections up to and including contributions of order c_k is given in analogy with Equation (31) in column form by:

$$S[\leq c_k] = \sum_{i=0}^k S^{c_i} = (\tilde{\Omega}^0 + \tilde{\Omega} + \tilde{\Omega}^2 + \dots + \tilde{\Omega}^k) \otimes S^{c_0}(E_p), \quad (35)$$

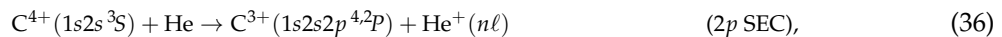
where each cross section entry i of the column vector S^{c_k} can be symbolised by $\sigma_i^{c_k}$.

The simplicity of this matrix formulation is obvious. One only needs to compute the partial fluorescence yields ω_{if} for all relevant transitions and insert them into the matrix $\tilde{\Omega}$ and, of course, to have also calculated the relevant direct (0-th order) cross sections $S^{c_0}(E_p)$ at each collision energy E_p . Then, all available cascade orders may be readily computed for all required levels using Equation (34).

The results of our cascade calculations based on such an iterative cascade matrix formulation have already been presented in Ref. [30]. The details of our matrix approach, presented here for the first time, are seen to be similar to other cascade matrix formulations that appear in the literature, as for example in the analysis of optical recombination line spectra by astrophysicists (see [3,47] and references therein). Our upper triangular matrix $\tilde{\Omega}$ consisting of the RBRs, is seen to be equivalent to the full cascade matrix $C_{nl,n'l'}$ for any transition from level n, l to any other n', l' [47]. Indeed, in the cascade matrix $C_{nl,n'l'}$ only transitions from higher-lying energy levels to lower-lying levels have non-zero RBRs, thus making it equivalent to an upper triangular matrix. Our formulation, independently derived as an extension of the diagrammatic approach of Curtis [38], seems to be simpler and mathematically more transparent, allowing for the direct calculation of any cascade order.

3. Calculations of $1s2s2p\ ^4P$ and 2P SEC Populations Including Cascade Repopulation

As mentioned earlier, in the production of the $1s2s2p\ ^4P$ and $1s2s2p\ ^2P$ states by $2p$ SEC in collisions of He-like ($1s2s\ ^3S$) ion beams with atomic targets, as for example in:



it has been shown that the production of the $1s2s2p\ ^4P$ population is enhanced relative to the 2P populations [33,34] due to *selective* cascade feeding [30,35]. As shown schematically in Figure 2, higher-lying $1s2sn\ell\ ^4L$ quartet states (with $n > 2$ and $L = \ell \leq n - 1$), also formed in the collision by $n\ell$ SEC, Auger decay very *weakly* to the $1s^2$ ground state (forbidden by spin conservation), compared to the corresponding higher-lying $1s2sn\ell\ ^2L$ doublet states, similarly formed in the collision, which *strongly* Auger decay to the $1s^2$ ground state (allowed by spin conservation). Both quartets and doublets also strongly radiatively decay to lower-lying quartets and doublets correspondingly, thus, in principle, cascade feeding all lower-lying states of the *same* spin symmetry (intercombination quartet \rightleftharpoons doublet E1 transitions are spin forbidden [48,49] and thus very weak). However, in practice, the doublets are efficiently depleted by their much stronger Auger decay allowing for minimal cascade feeding of lower-lying doublet levels, while quartets suffer negligible Auger depletion, thus resulting in strong cascade repopulation. Eventually, practically all higher-lying quartet SEC population is effectively transferred to the $1s2s2p\ ^4P$ state which is thus seen to act as a kind of “excited” ground state [30,33–35].

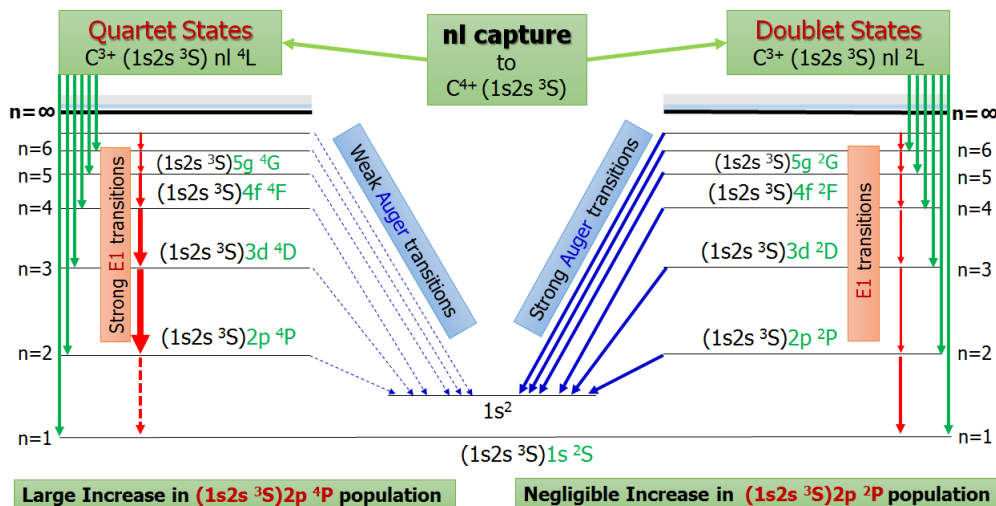


Figure 2. Schematic illustration of the $1s2s2p^4P$ state selective cascade feeding mechanism compared to the similarly configured $1s2s2p^2P$ states all produced by SEC in collisions of $C^{4+}(1s2s^3S)$ with atomic targets. Green solid arrows: nl SEC leading to the production of $1s2snl^4L$ quartets (left) and $1s2snl^2L$ doublets (right). Red arrows: E1 radiative transitions. Blue arrows: Auger transitions to $C^{4+}(1s^2)$ ground state. The strong Auger decay of the doublet states (solid blue slanted arrows) depletes their SEC populations resulting in negligible cascade feeding of the $1s2s2p^2P$ state. On the contrary, the much weaker Auger decay of the quartet states (dashed blue slanted arrows - forbidden due to spin conservation) allows for the strong cascade feeding of the $1s2s2p^4P$ state.

Consequently, to determine the direct $2p$ SEC cross section in the production of the $1s2s2p^4P$ and $2p$ states according to Equation (36), as well as their ratio R , one must also separately determine the cascade contributions. Since this usually cannot be done experimentally, it is typically included in the calculation. This requires the additional cascade calculation, as presented in Section 2, which includes the atomic structure calculation of the necessary RBRs, as well as the collision dynamics calculations of the initial production cross sections. Next, we present our RBR results based on the COWAN code calculations, as well as the initial production cross sections based on our 3eAOCC approach.

3.1. Decay Rates and Radiative Branching Ratios for $C^{3+}[(1s2s^3S)nl^{4,2L}]$ States with $n = 3$ and $n = 4$

Reported atomic structure calculations on Li-like ion states including carbon have been quite prevalent. In particular, the energies of the $1s^2nl^l$ states for $n = 2, 3$ and their E1 and Auger transition rates to $1s^2nl$ and $1s^2$, respectively have been reported by Cheng [50] and Chen [51] using the multi-configuration Dirac-Fock method (MCDF). Also by Vainshtein and Safronova [52], Safronova and Bruch [53], and most recently by Goryaev et al. [54], using the Z-expansion method. Davis and Chung [55] presented results for the spin-induced autoionization and radiative transition rates for the $1s2s2p^4P_j$ states using the saddle-point complex rotation method. More recently, radiative and Auger transition rates also using the MCDF method, were presented for $1s2s2p^4P_j$ states by Benis et al. [56] and for $1s2s3p$ levels by Santos et al. [57].

In addition, various energy level calculations, Auger yields and line identifications of Auger transitions for Li-like carbon states have also been presented within the field of high resolution Auger projectile spectroscopy in ion-atom collisions by Schneider et al. [24,58], Mann [59], Mack and Niehaus [44], and Deveney et al. [60]. In all these publications, radiative transitions to the singly excited states $1s^2nl$ are only reported. However, some selective results on carbon, for radiative transitions between doubly excited states are given in Blanke et al. [61,62] (including lifetimes of $1s2pnl^4L$ states for $n = 2 - 3$), [62] (wavelengths of $1s2s3d^4D \rightarrow 1s2s2p^4P$ transitions), Laughlin [63] (transition rates and radiative lifetimes for $1s2snl^4L$ and $1s2pnl^4L$ levels with $L \leq 4$). These results do not cover all the radiative and Auger transitions needed for our cascade calculations. We therefore performed our

own calculations using the COWAN code [39], to obtain the radiative and Auger transition rates and RBRs for the $C^{3+}[(1s2s^3S)n\ell^2 4L]$ states decaying to the $1s2sn'l' 2^4L'$ states. These results were used in our present calculations of the cascade repopulation of the $1s2s2p^2 4P$ states during the capture process.

Our calculations were carried out using the 2018 version of the COWAN [39] code, which is free of certain bugs reported earlier [64]. Our results on transition rates were compared with data from Ref. [51] for $n = 2$ and $n = 3$ and found in good agreement. The RCE subroutine of the code that performs the least-squares fitting of the energy levels was not used due to the lack of an adequate number of experimentally determined energy levels for the $C^{3+}[(1s2s^3S)n\ell^2 4L]$ states.

For the autoionizing decays of the $C^{3+}(1s2sn\ell)$ configurations with $n \leq 6$, the only allowed final state is the ground state $1s^2 1S$ of C^{4+} [41]. Thus, the Auger decay channels reported here correspond to transitions $1s2sn\ell (2S+1)L_J \rightarrow 1s^2 1S_0 + e^-(l)$. Moreover, our results include Auger decay rates for transitions that violate spin conservation (i.e., $\Delta S \neq 0$) for the Coulomb interaction, e.g., $(1s2s^3S)3p^4 P_{1/2} \rightarrow 1s^2 1S_0 + e^-(p)$. Such transitions are attributed to the fact that the initial state of the transition is a mixed-state, i.e., it cannot be represented as a pure state in the LS coupling scheme, and thus decays via a component of the mixed-state that is permitted to Auger decay [55].

Our results for the decay rates and branching ratios are presented in Table 1 for the quartet and Table 2 for the doublet states, respectively. Transitions with RBRs smaller than 0.1 are considered negligible and omitted. Based on these results, a Grotrian diagram of the strongest quartet transitions for the carbon $1s2sn\ell 4L_J$ states with $n \leq 4$ is shown in Figure 3.

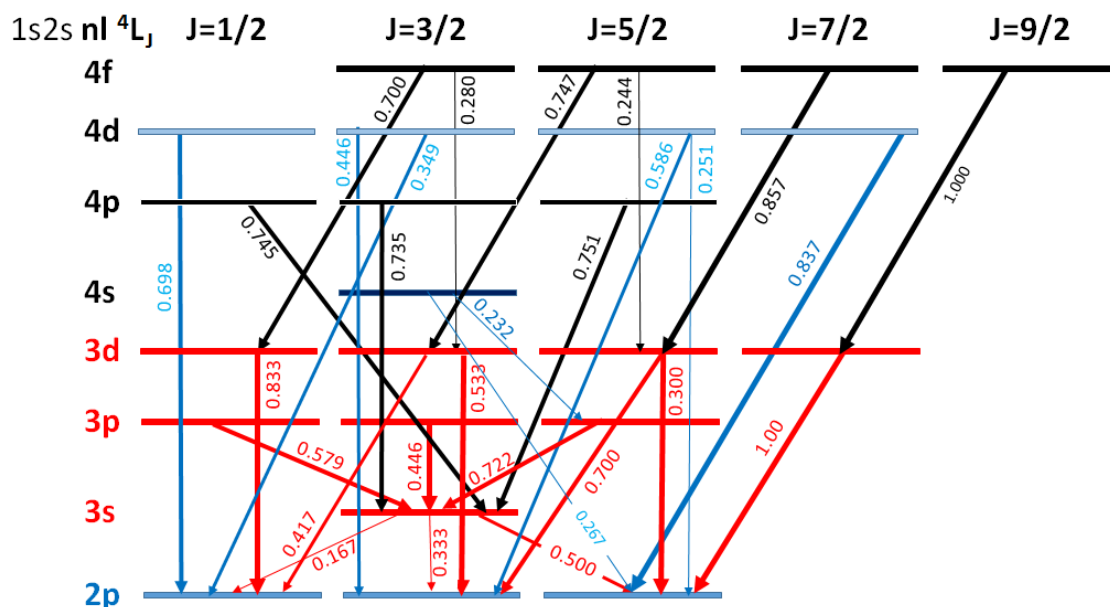


Figure 3. Grotrian diagram of the $C^{3+}(1s2sn\ell 4L)$ quartet level system for $n \leq 4$. E1 transition selection rules require $\Delta l = \pm 1, \Delta J = 0, \pm 1$ and $\Delta S = 0$. Only E1 transitions with the strongest RBRs from Table 1 are shown. The c_2 Yrast transition chain $4f^4 F_{9/2} \rightarrow 3d^4 D_{7/2} \rightarrow 2p^4 P_{5/2}$ is clearly seen to have the strongest branching ratios.

Table 1. Radiative (A_{ij}^r) and Auger ($A_{if'}^a$) decay rates, radiative branching ratios (RBR) given by the partial fluorescence yields (ω_{ij}), and partial Auger yields ($\zeta_{if'}$) for selected transitions of the $C^{3+}[(1s2s^3S)nl^4L]$ quartet states for $n = 2 - 4$. States are listed in order of decreasing binding energy. The lowest-lying levels (of primary interest) are separated from the rest by a double line. A “-” signifies that the computed rate leads to a negligible value (i.e., <0.1) for the related partial branching ratio and is therefore not listed.

<i>i</i> #	Initial <i>nl</i> $2S+1L_J$	<i>j</i> #	Final ^a <i>nl</i> $2S+1L_J$	$A_{ij}^r (s^{-1})$	$A_{if'}^a (s^{-1})$ ^a	$\alpha_i (s^{-1})$ (Equation (2))	RBR— ω_{ij} (Equation (4))	$\zeta_{if'}$ ^a (Equation (5))
1	$2p^4P_{1/2}$	-	-	-	3.39×10^8 ^b	3.401×10^8 ^b	-	0.996
2	$2p^4P_{3/2}$	-	-	-	1.37×10^8 ^b	1.374×10^8 ^b	-	0.997
3	$2p^4P_{5/2}$	-	-	-	8.26×10^6 ^b	8.239×10^6 ^b	-	0.998
4	$3s^4S_{3/2}$	1	$2p^4P_{1/2}$	3.038×10^9	-	1.820×10^{10}	0.167	-
4		2	$2p^4P_{3/2}$	6.071×10^9	-		0.333	-
4		3	$2p^4P_{5/2}$	9.095×10^9	-		0.500	-
5	$3p^4P_{1/2}$	4	$3s^4S_{3/2}$	8.643×10^7	2.730×10^7	1.492×10^8	0.579	0.183
6	$3p^4P_{3/2}$	4	$3s^4S_{3/2}$	1.733×10^8	1.380×10^8	3.886×10^8	0.446	0.355
7	$3p^4P_{5/2}$	4	$3s^4S_{3/2}$	2.611×10^8	-	3.615×10^8	0.722	-
8	$3d^4D_{1/2}$	1	$2p^4P_{1/2}$	4.661×10^{10}	-	5.595×10^{10}	0.833	-
8		2	$2p^4P_{3/2}$	9.316×10^9	-		0.167	-
9	$3d^4D_{3/2}$	1	$2p^4P_{1/2}$	4.661×10^{10}	3.240×10^5	1.119×10^{11}	0.417	-
9		2	$2p^4P_{3/2}$	5.962×10^{10}	-		0.533	-
9		3	$2p^4P_{5/2}$	5.584×10^9	-		0.050	-
10	$3d^4D_{5/2}$	2	$2p^4P_{3/2}$	1.174×10^{11}	7.590×10^5	1.677×10^{11}	0.700	-
10		3	$2p^4P_{5/2}$	5.026×10^{10}	-		0.300	-
11	$3d^4D_{7/2}$	3	$2p^4P_{5/2}$	2.234×10^{11}	-	2.235×10^{11}	1.000	-
12	$4s^4S_{3/2}$	2	$2p^4P_{3/2}$	1.875×10^9	-	1.051×10^{10}	0.178	-
12		3	$2p^4P_{5/2}$	2.810×10^9	-		0.267	-
12		6	$3p^4P_{3/2}$	1.630×10^9	-		0.155	-
12		7	$3p^4P_{5/2}$	2.442×10^9	-		0.232	-
13	$4p^4P_{1/2}$	4	$3s^4S_{3/2}$	1.214×10^9	1.280×10^7	1.630×10^9	0.745	-
13		8	$3d^4D_{1/2}$	1.866×10^8	-		0.114	-
13		9	$3d^4D_{3/2}$	1.866×10^8	-		0.114	-
14	$4p^4P_{3/2}$	4	$3s^4S_{3/2}$	2.427×10^9	6.460×10^7	3.302×10^9	0.735	-
14		10	$3d^4D_{5/2}$	4.703×10^8	-		0.142	-
15	$4p^4P_{5/2}$	4	$3s^4S_{3/2}$	3.642×10^9	-	4.850×10^9	0.751	-
15		11	$3d^4D_{7/2}$	8.960×10^8	-		0.185	-
16	$4d^4D_{1/2}$	1	$2p^4P_{1/2}$	1.614×10^{10}	-	2.314×10^{10}	0.698	-
16		2	$2p^4P_{3/2}$	3.225×10^9	-		0.139	-
16		5	$3p^4P_{1/2}$	3.141×10^9	-		0.136	-
17	$4d^4D_{3/2}$	1	$2p^4P_{1/2}$	1.614×10^{10}	1.560×10^5	4.626×10^{10}	0.349	-
17		2	$2p^4P_{3/2}$	2.064×10^{10}	-		0.446	-
18	$4d^4D_{5/2}$	2	$2p^4P_{3/2}$	4.064×10^{10}	3.640×10^5	6.936×10^{10}	0.586	-
18		3	$2p^4P_{5/2}$	1.740×10^{10}	-		0.251	-
18		6	$3p^4P_{3/2}$	7.911×10^9	-		0.114	-
19	$4d^4D_{7/2}$	3	$2p^4P_{5/2}$	7.735×10^{10}	-	9.243×10^{10}	0.837	-
19		7	$3p^4P_{5/2}$	1.506×10^{10}	-		0.163	-
20	$4f^4F_{3/2}$	8	$3d^4D_{1/2}$	1.153×10^{10}	-	1.647×10^{10}	0.700	-
20		9	$3d^4D_{3/2}$	4.614×10^9	-		0.280	-
21	$4f^4F_{5/2}$	9	$3d^4D_{3/2}$	1.845×10^{10}	7.060×10^4	2.471×10^{10}	0.747	-
21		10	$3d^4D_{5/2}$	6.025×10^9	-		0.244	-
22	$4f^4F_{7/2}$	10	$3d^4D_{5/2}$	2.824×10^{10}	1.290×10^5	3.295×10^{10}	0.857	-
22		11	$3d^4D_{7/2}$	4.706×10^9	-		0.143	-
23	$4f^4F_{9/2}$	11	$3d^4D_{7/2}$	4.118×10^{10}	-	4.118×10^{10}	1.000	-

^a All Auger transitions refer to the same final ionic state f' , i.e., $C^{4+}(1s^2 1S_0)$; ^b From Benis et al. [56].

Table 2. Same as Table 1, but for the $C^{3+}[(1s2s^3,^1S)nl^2L]$ doublet states. Shorthand: $nl^2L_{-J} \equiv (1s2s^3S)nl^2L_J$ and $nl^2L_{+J} \equiv (1s2s^1S)nl^2L_J$. Here we only list states with the largest radiative rates, as well as a few other indicative connecting ones. In most cases, the RBR is much smaller than 0.022, marked by "-" and considered negligible.

<i>i</i> #	Initial $nl^{2S+1}L_J$	<i>j</i> #	Final ^a $nl^{2S+1}L_J$	$A_{ij}^r(s^{-1})$	$A_{ij'}^a(s^{-1})^a$	$\alpha_i(s^{-1})$ (Equation (2))	RBR— ω_{ij} (Equation (4))	$\zeta_{ij'}^a$ (Equation (5))
1	$2p^2P_{-1/2}$	-	-	-	1.47×10^{13} ^b	1.52×10^{13} ^b	-	0.968
2	$2p^2P_{-3/2}$	-	-	-	1.43×10^{13} ^b	1.48×10^{13} ^b	-	0.967
3	$2p^2P_{+1/2}$	-	-	-	3.86×10^{13} ^b	3.87×10^{13} ^b	-	0.998
4	$2p^2P_{+3/2}$	-	-	-	3.86×10^{13} ^b	3.87×10^{13} ^b	-	0.998
5	$3s^2S_{-1/2}$	1	$2p^2P_{-1/2}$	2.954×10^8	2.380×10^{13}	2.381×10^{13}	-	1.00
5		2	$2p^2P_{-3/2}$	5.795×10^8			-	
5		3	$2p^2P_{+1/2}$	1.734×10^9			-	
5		4	$2p^2P_{+3/2}$	3.482×10^9			-	
6	$3s^2S_{+1/2}$	3	$2p^2P_{+1/2}$	2.084×10^9	1.380×10^{13}	1.382×10^{13}	-	0.999
7	$3p^2P_{-1/2}$	6	$3s^2S_{+1/2}$	1.561×10^7	5.130×10^{12}	5.494×10^{12}	-	0.934
8	$3p^2P_{-3/2}$	5	$3s^2S_{-1/2}$	3.107×10^7	1.030×10^{13}	1.103×10^{13}	-	0.934
9	$3p^2P_{+1/2}$	6	$3s^2S_{+1/2}$	4.573×10^7	1.880×10^{13}	1.893×10^{13}	-	0.993
10	$3p^2P_{+3/2}$	6	$3s^2S_{+1/2}$	9.235×10^7	3.760×10^{13}	3.785×10^{13}	-	0.993
11	$3d^2D_{-3/2}$	3	$2p^2P_{+1/2}$	4.768×10^{10}	5.690×10^{11}	6.751×10^{11}	0.071	0.843
12	$3d^2D_{-5/2}$	4	$2p^2P_{+3/2}$	8.646×10^{10}	8.540×10^{11}	1.013×10^{12}	0.085	0.843
13	$3d^2D_{+3/2}$	1	$2p^2P_{-1/2}$	4.480×10^{10}	1.830×10^{12}	1.937×10^{12}	0.023	0.945
14	$3d^2D_{+5/2}$	2	$2p^2P_{-3/2}$	8.120×10^{10}	2.740×10^{12}	2.901×10^{12}	0.028	0.945
15	$4s^2S_{-1/2}$	4	$2p^2P_{+3/2}$	1.716×10^9	9.530×10^{12}	9.536×10^{12}	-	0.999
16	$4s^2S_{+1/2}$	4	$2p^2P_{+3/2}$	1.920×10^9	4.780×10^{12}	4.792×10^{12}	-	0.997
17	$4p^2P_{-3/2}$	5	$3s^2S_{-1/2}$	3.251×10^9	4.020×10^{12}	4.369×10^{12}	-	0.920
18	$4p^2P_{+3/2}$	6	$3s^2S_{+1/2}$	2.667×10^9	1.510×10^{13}	1.519×10^{13}	-	0.994
19	$4d^2D_{-3/2}$	1	$2p^2P_{-1/2}$	1.865×10^{10}	2.130×10^{11}	2.627×10^{11}	0.071	0.811
20	$4d^2D_{-5/2}$	4	$2p^2P_{+3/2}$	2.507×10^{10}	3.190×10^{11}	3.936×10^{11}	0.064	0.810
21	$4d^2D_{+3/2}$	3	$2p^2P_{+1/2}$	2.477×10^{10}	1.040×10^{12}	1.084×10^{12}	0.022	0.960
22	$4d^2D_{+5/2}$	4	$2p^2P_{+3/2}$	4.442×10^{10}	1.550×10^{12}	1.615×10^{12}	0.028	0.960
23	$4f^2F_{-5/2}$	11	$3d^2D_{-3/2}$	2.081×10^{10}	5.170×10^9	2.835×10^{10}	0.734	0.182
24	$4f^2F_{-7/2}$	12	$3d^2D_{-5/2}$	2.973×10^{10}	6.890×10^9	3.780×10^{10}	0.787	0.182
25	$4f^2F_{+5/2}$	13	$3d^2D_{+3/2}$	2.241×10^{10}	6.550×10^9	3.186×10^{10}	0.703	0.206
26	$4f^2F_{+7/2}$	14	$3d^2D_{+5/2}$	3.201×10^{10}	8.730×10^9	4.247×10^{10}	0.754	0.206

^a All Auger transitions refer to the same final ionic state, i.e., $C^{4+}(1s^2\ ^1S_0)$; ^b From Chen [51].

3.2. Cascade Feeding Considerations

As seen in Table 1 and more clearly in the Grotrian diagram of Figure 3 for the quartets, there are higher-lying levels where the RBR ω_{ij} is close to 1. On the other hand, in Table 2 for the doublets, the computed RBRs are mostly very small making cascade feeding negligible. This is consistent with previous cascade repopulation findings for Li-like carbon [34,35] and fluorine [33] states populated by nl SEC (Equation (36)). Therefore, in the case of the doublets, *no cascade* calculations were performed. Thus, cascade feeding calculations were only performed for the quartet states.

In general, for the quartets, the Auger rates A_{if}^a decrease in strength as the principal quantum number n increases, while the radiative rates A_{ij}^r increase. Thus, the higher-lying levels are seen to have increased RBRs compared to levels below them, increasing the cascade feeding probability of the lowest-lying $2p^4P_J$ levels (i.e., with $J = 1/2, 3/2, 5/2$) of interest. Of special interest are also the Yrast

states (those with maximal J within the same nl^4L level), as already pointed out by Schneider et al [24], which can provide a path of maximal cascade probability. Indeed, we note that the Yrast cascade chain $4f^4F_{9/2} \rightarrow 3d^4D_{7/2} \rightarrow 2p^4P_{5/2}$ (or in Table 1 level numbers $23 \rightarrow 11 \rightarrow 3$) all have the strongest RBRs $\omega_{if} = 1$ along this path (e.g., $\omega_{23,11} = \omega_{11,3} = 1$) and therefore a 2nd-order (c_2) cascade probability of 1 ($\omega_{23,11} \cdot \omega_{11,3} = 1$).

For the doublets, even though there are RBRs with large ω_{ij} values as listed in Table 2 for $n = 4$ (e.g., the Yrast transition $4f^2F_{-7/2} \rightarrow 3d^2D_{-5/2}$, has $\omega_{24,12} = 0.787$), their follow up transition feeding the levels of interest are seen to be much weaker (e.g., the transition $3d^2D_{-5/2} \rightarrow 2p^2P_{+1/2}$, has only $\omega_{12,3} = 0.085$), effectively resulting in a negligible overall c_2 cascade probability (e.g., $0.787 \cdot 0.085 = 0.067$).

3.3. Initial State Populations

The same initial state populations (cross sections $S^{co}(E_p)$ in Equation (33)) were used as used in Ref. [30]. These were computed in [30] for $2p$ SEC using ab initio dynamical calculations involving *three* active electrons within a full configuration interaction approach. This involved a semiclassical atomic orbital close-coupling calculation (referred to as 3eAOCC), with asymptotic descriptions of the atomic collision partners [65–67]: the time-dependent Schrödinger equation was solved non-perturbatively, with the inclusion of all couplings related to the static and dynamic interelectronic repulsions and effects stemming from the Pauli exclusion principle. This approach allows for the accurate modeling of the C^{4+} and C^{3+} electronic structures, including spin and spatial components. It also describes the dynamics of the system, inducing among other things, excitation, ionization (through population of pseudo states [67]) and capture to singly and doubly excited states on the carbon center. Overall, this 3eAOCC approach goes much beyond frozen core models advocated in the past [34,35], where only *one* active electron is considered in the dynamics⁴. SEC cross sections to higher-lying $1s2snl^4L$ states for $n = 3 - 4$ were also computed by our close-coupling treatment. Finally, the He target was described by a model potential binding just a *single* electron to He^+ with the appropriate $He(1s^2)$ energies⁴.

Using these initial state cross sections, the calculated ratio R was found in good agreement with experiment, for the first time, when the radiative cascades were also taken into account. These results on R , presented in [30], resolved the previously existing disagreement between theory and experiment [34,35], while underlining the limited predictive power of the frozen core approximation as regards to spin statistics in such highly correlated dynamical atomic systems.

4. Results and Discussion

In this work, we implement the cascade matrix formulation (i.e., Equation (34)), progressively computing increasing cascade order contributions to obtain the overall cascade repopulation of the states of interest. This requires the independent calculation of: (i) the initial SEC production cross sections, and (ii) the necessary RBRs ω_{ij} . Since, as already mentioned, intercombination transitions are very weak, the cascade calculations are typically done separately for each spin symmetry (i.e., quartet or doublet). Due to the much smaller doublet RBRs (compared to the corresponding quartet RBRs), as evident in Table 2, the cascade repopulation of the doublets will be insignificant, consistent with previously reported results [35], and is therefore not performed. Thus, only cascade repopulation of the quartet states is considered here. This is performed using an $\tilde{\Omega}[M = 23 \times M = 23]$ cascade matrix with entries $\tilde{\omega}_{ji} = \omega_{ij}$, as listed in Table 1.

⁴ See [30] Supplemental Material at <http://link.aps.org/supplemental/10.1103/PhysRevLett.124.113401> for additional details on the theoretical 3eAOCC approach

4.1. Cascade Enhancement of the $1s2s2p^4P$ Level Population and Contributing Cascade Orders

In Figure 4, we plot, as a function of the collision energy E_p , the ratio of progressive cascade contributions c_1 , c_2 , and c_3 to c_0 for the $1s2s2p^4P$ state due to higher-lying $1s2sn\ell^4L$ populations with increasing principal quantum number n .

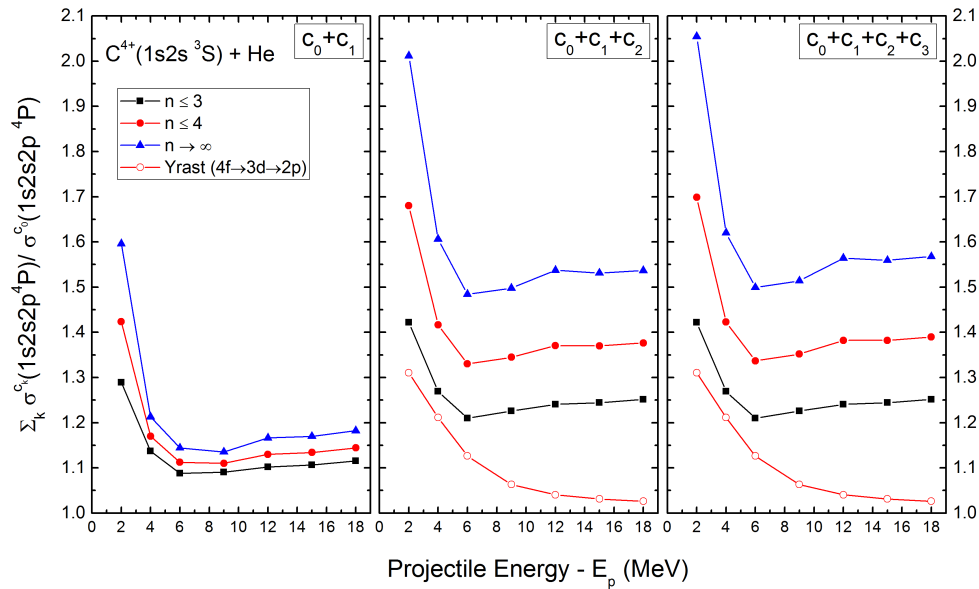


Figure 4. Ratio of the cumulative cascade contributions of the $1s2sn\ell^4L$ state populations to the $1s2s2p^4P$ as a function of the projectile energy E_p , for increasing principal quantum number n . Cascade contributions including up to: [Left] first order, c_1 . [Middle] second order, c_2 . [Right] third order, c_3 . Symbols: (Black squares) $n \leq 3$, (Red circles) $n \leq 4$, (Blue triangles) Extrapolation to include all $n \rightarrow \infty$. Convergence is seen to be attained with c_3 . The Yrast c_2 contribution (Red open circles) $4f^4F_{9/2} \rightarrow 3d^4D_{7/2} \rightarrow 2p^4P_{5/2}$ (see text) is also shown for comparison.

These results are then extrapolated to $n \rightarrow \infty$, using an n^{-3} SEC population model [34,45]. From Figure 4, it is evident, that depending on collision energy E_p , the first cascade order c_1 , accounts for an increase of about 10–30% for transitions just from the $n = 3$ levels. This is consistent with the Grotrian diagram in Figure 3, where most $n = 3$ RBRs are seen to be large. Furthermore, the second cascade order, c_2 , for both $n = 3$ and $n = 3 + 4$, as well as the extrapolation to include all n , are even more important accounting for a further increase of 10–40%. Finally, including also cascade contributions c_3 , only a very small increase is observed with decreasing collision energy, as SEC to higher-lying n levels becomes more important [44]. Also shown, is the contribution of the Yrast cascade sequence also seen to become increasingly important with decreasing collision energy.

4.2. Spin Statistics—Ratio R of $1s2s2p^4P$ to $2P$ Cross Sections

In our recent publication [30], the long-standing problem of how multi-unpaired-electron ion cores behave, while undergoing electron processes during fast atomic collisions, was treated both experimentally and theoretically. A viable way to explore this is to consider the $2p$ SEC channel in MeV collisions (Equation (36)). There, the ratio R of the similarly configured $1s2s2p^4P$ to $2P_{\pm}$ SEC cross sections, defined by Equation (37), should bear the corresponding population spin statistics signature. This ratio should have the value of $R = 1$ when considering only spin multiplicity, or the value $R = 2$, in the frozen core approximation, where only the $4p$ and a single $2p$ states can be produced by SEC from the $1s2s^3S$ initial state [34,36,37]. Experimental investigations involved beams of $C^{4+}(1s^2, 1s2s^3S)$ mixed-state ions, prepared with different amounts of metastable $1s2s^3S$ component. Then, the ratio R could be evaluated by applying our two-spectra technique for the proper determination of the contributions from just the $1s2s^3S$ beam component [43]. The measurements were performed using

the ZAPS [46] setup, currently located at the NCSR “Demokritos” 5.5 MV Tandem accelerator facility in Athens [68]. The corresponding theoretical investigations were performed in Paris using the above mentioned 3eAOCC calculations involving the dynamics of *three active* electrons within a full configuration interaction approach [66].

Based on the above 3eAOCC and cascade calculations, the ratio R of the SEC cross sections of the quartet $1s2s2p\ ^4P$ (for short 4P) to doublet $1s2s2p\ ^2P_{\pm}$ (for short $^2P_{\pm}$) is given by:

$$R \equiv \frac{\sigma(^4P)}{\sigma(^2P_-) + \sigma(^2P_+)} = \frac{\sigma^{c_0}(^4P) + \sigma^{c_1}(^4P) + \sigma^{c_2}(^4P) + \sigma^{c_3}(^4P)}{\sigma^{c_0}(^2P_-) + \sigma^{c_0}(^2P_+)}, \quad (37)$$

where the cross sections $\sigma^{c_k}(X)$ correspond to the sum of the cross sections of all levels i related to the same term X , e.g., $\sigma^{c_3}(^4P) = \sigma^{c_3}(^4P_{1/2}) + \sigma^{c_3}(^4P_{3/2}) + \sigma^{c_3}(^4P_{5/2})$, i.e., the c_3 cascade contributions to levels $i = 1 - 3$ according to Table 1.

R was computed up to and including third order cascades, c_3 , according to the formulation of Equation (34). Results are shown in Figure 5, along with the ZAPS measurements reported in [30]. Here, we increased the number of electron configurations from 20 to 29 in the COWAN code⁵ obtaining slightly smaller values for R compared to the ones previously reported [30], which resulted in improved agreement with experiment as seen in Figure 5.

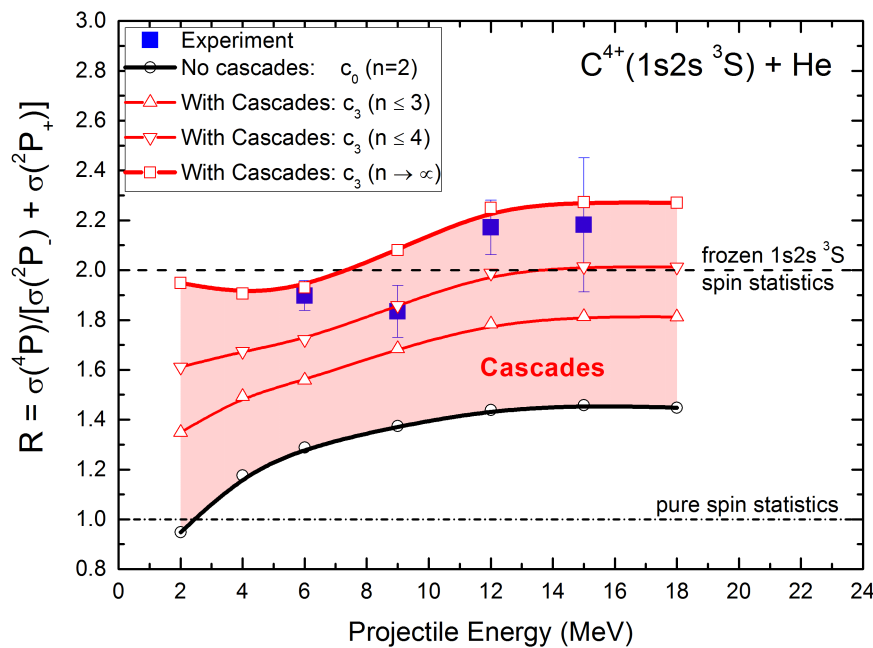


Figure 5. Ratio R of $1s2s2p\ ^4P$ to $1s2s2p\ ^2P_{\pm}$ cross sections in collisions of $C^{4+}(1s2s\ ^3S)$ ions with He as a function of the projectile energy (see Equation (37)). Experiment: Blue squares [30]. Calculations (3eAOCC [30]): Black line and open circles (no cascades $n=2$, only c_0 possible); Red lines including cascades up to c_3 (see Equation (34)). Triangles: $n \leq 3$; Inverted triangles: $n \leq 4$; Open squares: Includes all $n \rightarrow \infty$ (extrapolations based on an n^{-3} model). The cascade contributions (shaded region) are thus seen to enhance the ratio R over and above its direct $2p$ SEC value (black line). The frozen $1s2s\ ^3S$ core spin statistics and pure spin statistics values are also indicated. The cascade calculations shown here include a more extensive number of configurations than what was used in Ref. [30] (see text) and show slightly improved agreement with experiment.

⁵ New calculations (this work): 29 configurations consisting of $1s2snl$ ($n = 2, 3, 4, 5$) + $1s^2nl$ ($n = 2, 3, 4, 5$) + $1s2p^2$. Previous calculations ([30]): 20 configurations consisting of $1s2snl$ ($n = 2, 3, 4$) + $1s^2nl$ ($n = 2, 3$) + $1s2p^2$ + $1s3snl$ ($n = 2, 3$).

These and our previous results [30], essentially invalidate the frozen core approximation commonly used in the past (e.g., Röhrbein et al. [35], found much larger values of the ratio R with or without cascades) when considering electron capture in multi-electron, multi-open-shell quantum systems [30]. While the frozen $1s2s^3S$ spin statistic limit shown in Figure 5 with the value of 2 [37], does indeed seem to agree with our experimental data, it does *not* include cascades. These have been shown by us (and Röhrbein et al. [35] before us) to be important, lifting this limit of 2 to about 3.5 (minimum), when including cascade repopulation as calculated here.

4.3. Comparison to Older Cascade Calculations on the $C^{4+}(1s2s^3S)+He$ Collision System

Finally, we should also mention the two previous cascade calculations for the same $C^{4+}(1s2s^3S)+He$ collision system reported by Strohschein et al. [34] and Röhrbein et al. [35]. In Ref. [34], the cascade calculations ignored the Auger channel. Thus, the decay constant α_n in Equation (2) included only radiative rates and was therefore smaller than when Augers are included. This was corrected in Ref. [35], where the full α_n decay constants were used, thus also properly including the Auger decays. In the former 4P calculation [34], since the 4P Auger decay rate is small compared to the inter-quartet $E1$ radiative transitions rates, the RBR is not much affected by the non-inclusion of the Auger channel, so the selective enhancement of the 4P remained substantial [34]. However, neglecting the Auger channel in the calculation of the doublets is a much stronger effect since here the RBRs change substantially [35]. This can be readily seen in our calculated doublet rates shown in Table 2. For example, for the initial level $(1s2s^3S)3d^2D_{5/2}$, referred to in the table as level 12 ($3d^2D_{-5/2}$), $\alpha_{12} = 1.013 \times 10^{12} \text{ s}^{-1}$ including the Auger channel, while equal to $1.013 \times 10^{12} - 8.540 \times 10^{11} = 1.590 \times 10^{11} \text{ s}^{-1}$ without, with corresponding RBR $\omega_{12,4} = 8.646 \times 10^{10} / 1.103 \times 10^{12} = 0.0854$ with the Auger channel, and $\omega_{12,4} = 8.646 \times 10^{10} / 1.590 \times 10^{11} = 0.5438$ without (a huge difference).

In addition to these atomic structure considerations, in both previous calculations, the initial SEC populations were calculated within a one-active-electron frozen core treatment using the two-center basis generator method (TC-BGM) [35]. This gave a ratio $R \approx 2$ without cascades, very different from the value of $R \approx 1.1 - 1.4$ reported by us [30], using the 3eAOCC approach. Furthermore, the cascade contributions to R were found to increase its value by a factor of $\lesssim 2.9$ (see Figure 6 in Ref. [35]), while in our calculation [30], as also shown here, the increase due to cascades in R is smaller, at about a factor ~ 1.6 (see Figure 5). These differences between the two results, can be readily attributed in both cases (i.e., R with and without cascade contributions) to the present use of a dynamic approach involving several active correlated electrons, avoiding the constraints of the $1s2s^3S$ frozen core approximation required in one-electron treatments [30].

5. Summary and Conclusions

We have theoretically investigated radiative cascade repopulation of the $C^{3+}(1s2s^2p)^4P$ quartet and 2P doublet states formed in 2–18 MeV collisions of $C^{4+}(1s2s^3S)$ ions with He gas target. Using the diagrammatic cascade formalism of Curtis [38], after including also the Auger decay of the doubly excited states, we have integrated the rate equations over long-enough time ($t \rightarrow \infty$) to obtain the final level populations including cascade repopulation. Results are calculated analytically within a straight-forward cascade matrix approach and the contributions of each cascade order to the cross sections are readily computed, as described in detail.

To initiate the cascade calculations, the $t = 0$ initial populations of the $1s2snl^4L$, $1s2snl^2L$ levels included in our analysis are obtained from the direct nl single electron capture (SEC) cross sections previously computed in Ref. [30], using the novel three-electron close-coupling (3eAOCC) approach.

Our cascade matrix includes all relevant radiative branching ratios (RBR) for $n \leq 4$ computed using the COWAN atomic structure code. In the case of the doublets, the RBRs are found to be very small (< 0.1) showing that cascade feeding in this case, can be neglected, consistent with previous results by other groups [35]. In the case of the quartets though, the RBRs are found to be large, in some cases equal to 1. Cascade calculations (extrapolated to $n \rightarrow \infty$ using an n^{-3} SEC model) were then

performed including up to third order cascades, which showed an up to 60% increase of the $1s2s2p^4P$ population due to cascades. Using these cascade calculations including initial level populations provided by our independently calculated cross sections, we computed the ratio R of $1s2s2p^4P$ to $2P$ cross sections including cascades, of recent spin statistics interest [30,33–35], and found it in good agreement with experiment.

Future systematic isoelectronic investigations of the spin statistics ratio R would be of great interest to further validate our conclusions in a more general context. Cascade calculations will therefore also be important, particularly at the lowest collision energies where SEC to higher-lying levels is strongest.

Author Contributions: E.P.B. and T.J.M.Z. conceived, designed, participated in the experiments and prepared the manuscript; I.M., A.L. and S.N. (Stefanos Nanos) participated in the experiments and the data analysis; A.D. performed the 3eAOCC calculations; T.J.M.Z. developed the upper triangular matrix cascade formalism and computed the cascade contributions; S.N. (Sofoklis Nikolaou) and E.P.B. performed the COWAN transition rate calculations. All authors have read and agreed to the published version of the manuscript.

Funding: We acknowledge support by the project “Cluster of Accelerator Laboratories for Ion-Beam Research and Applications—CALIBRA” (MIS 5002799) which is implemented under the Action “Reinforcement of the Research and Innovation Infrastructure,” funded by the Operational Programme “Competitiveness, Entrepreneurship and Innovation” (NSRF 2014–2020) and co-financed by Greece and the European Union (European Regional Development Fund). T.J.M.Z. and A.D. also acknowledge support from the LABEX PLAS@PAR under Grant No. ANR-11-IDEX-0004-02.

Acknowledgments: We thank the staff of the Demokritos tandem accelerator for their help in day to day operational matters and during beam times and for the encouragement and support of the CALIBRA principal investigator Sotirios Harissopoulos.

Conflicts of Interest: The authors declare no conflict of interest.

References

1. Beiersdorfer, P. Laboratory X-ray Astrophysics. *Annu. Rev. Astron. Astrophys.* **2003**, *41*, 343–390. [[CrossRef](#)]
2. Shevelko, V.; Tawara, H. (Eds.) *Atomic Processes in Basic and Applied Physics*; Springer: Berlin/Heidelberg, Germany; New York, NY, USA, 2012.
3. Osterbrock, D.E.; Ferland, G.J. *Astrophysics of Gaseous Nebulae and Active Galactic Nuclei*; University Science Books: Mill Valley, CA, USA, 2006.
4. Pradhan, A.K.; Nahar, S.N. *Atomic Astrophysics and Spectroscopy*; Cambridge University Press: Cambridge, UK, 2011.
5. Bureyeva, L.A.; Lisitsa, V.S.; Namba, C.; Shuvaev, D.A. Radiative cascade following dielectronic recombination. *J. Phys. B* **2002**, *35*, 2505–2514. [[CrossRef](#)]
6. Cumbee, R.S.; Mullen, P.D.; Lyons, D.; Shelton, R.L.; Fogle, M.; Schultz, D.R.; Stancil, P.C. Charge Exchange X-ray Emission due to Highly Charged Ion Collisions with H, He, and H₂: Line Ratios for Heliospheric and Interstellar Applications. *Astrophys. J.* **2017**, *852*, 7. [[CrossRef](#)]
7. Fritzsche, S. A fresh computational approach to atomic structures, processes and cascades. *Comput. Phys. Commun.* **2019**, *240*, 1–14. [[CrossRef](#)]
8. Hahn, Y.; Lagattuta, K.J. Dielectronic recombination and related resonance processes. *Phys. Rep.* **1988**, *166*, 195–268. [[CrossRef](#)]
9. Pradhan, A.K. Recombination-cascade X-ray spectra of highly charged helium-like ions. *Astrophys. J.* **1985**, *288*, 824–830. [[CrossRef](#)]
10. Kabachnik, N.M.; Fritzsche, S.; Grum-Grzhimailo, A.N.; Meyer, M.; Ueda, K. Coherence and correlations in photoinduced Auger and fluorescence cascades in atoms. *Phys. Rep.* **2007**, *451*, 155–233. [[CrossRef](#)]
11. Loch, S.D.; Pindzola, M.S.; Ballance, C.P.; Griffin, D.C. The effects of radiative cascades on the X-ray diagnostic lines of Fe¹⁶⁺. *J. Phys. B* **2006**, *39*, 85–104. [[CrossRef](#)]
12. Mirakhdov, M.N.; Parilis, E.S. Auger and X-ray cascades following inner-shell ionisation. *J. Phys. B* **1988**, *21*, 795–804. [[CrossRef](#)]
13. Pepino, R.; Kharchenko, V.; Dalgarno, A.; Lallement, R. Spectra of the X-ray Emission Induced in the Interaction between the Solar Wind and the Heliospheric Gas. *Astrophys. J.* **2004**, *617*, 1347–1352. [[CrossRef](#)]

14. Trassinelli, M.; Prigent, C.; Lamour, E.; Mezdari, F.; Mérot, J.; Reuschl, R.; Rozet, J.P.; Steydli, S.; Vernhet, D. Investigation of slow collisions for (quasi) symmetric heavy systems: what can be extracted from high resolution X-ray spectra. *J. Phys. B* **2012**, *45*, 085202. [[CrossRef](#)]
15. Tawara, H.; Richard, P.; Safronova, U.I.; Stancil, P.C. K X-ray production in H-like Si¹³⁺, S¹⁵⁺, and Ar¹⁷⁺ ions colliding with various atom and molecule gas targets at low collision energies. *Phys. Rev. A* **2001**, *64*, 042712. [[CrossRef](#)]
16. Tawara, H.; Richard, P.; Safronova, U.I.; Stancil, P.C. Erratum. *Phys. Rev. A* **2002**, *65*, 059901. [[CrossRef](#)]
17. Astner, G.; Curtis, L.J.; Liljeby, L.; Mannervik, S.; Martinson, I. A high precision beam-foil meanlife measurement of the $1s3p^1P$ level in He I. *Zeitschrift Phys. A* **1976**, *279*, 1–6. [[CrossRef](#)]
18. Träbert, E. Beam-foil spectroscopy—Quo vadis? *Physica Scr.* **2008**, *78*, 038103. [[CrossRef](#)]
19. Curtis, L.J. *Beam Foil Spectroscopy*; Bashkin, S., Ed.; Springer: Berlin, Germany, 1976; p. 63.
20. Charalambidis, D.; Brenn, R.; Koulen, K.J. Transition rates of $1s2s2p^4P^o$ states of Li-like ions ($Z = 8, 7, 6$). *Phys. Rev. A* **1989**, *40*, 2359–2364. [[CrossRef](#)]
21. Träbert, E. Radiative-Lifetime measurements on highly charged Ions. In *Accelerator-Based Atomic Physics: Techniques and Applications*; Shafroth, S.M., Austin, J.C., Eds.; AIP: Woodbury, NY, USA, 1997; pp. 567–607; Chapter 17.
22. Träbert, E. In pursuit of highly accurate atomic lifetime measurements of multiply charged ions. *J. Phys. B* **2010**, *43*, 074034. [[CrossRef](#)]
23. Martinson, I. Mean life studies in light atoms. *Nucl. Instrum. Methods* **1970**, *90*, 81–84. [[CrossRef](#)]
24. Schneider, D.; Bruch, R.; Schwarz, W.H.E.; Chang, T.C.; Moore, C.F. Identifications of Auger spectra from 2-MeV foil-excited carbon ions. *Phys. Rev. A* **1977**, *15*, 926–934. [[CrossRef](#)]
25. Sellin, I.A.; Pegg, D.J.; Brown, M.; Smith, W.W.; Donnally, B. Spectra of Autoionization Electrons Emitted by Fast, Metastable Beams of Highly Stripped Oxygen and Fluorine Ions. *Phys. Rev. Lett.* **1971**, *27*, 1108–1111. [[CrossRef](#)]
26. Donnally, B.; Smith, W.W.; Pegg, D.J.; Brown, M.; Sellin, I.A. Lifetimes of the Metastable Auto-Ionizing ($1s2s2p^4P_{5/2}$) States of Lithiumlike F⁶⁺ and O⁵⁺ Ions. *Phys. Rev. A* **1971**, *4*, 122–125. [[CrossRef](#)]
27. Berry, H.G.; Pinnington, E.H.; Subtil, J.L. Energies and Mean Lives of Doubly Excited Terms in Lithium. *J. Opt. Soc. Am.* **1972**, *62*, 767–771. [[CrossRef](#)]
28. Sellin, I.A.; Pegg, D.J.; Griffin, P.M.; Smith, W.W. Metastable Autoionizing States of Highly Excited Heavy Ions. *Phys. Rev. Lett.* **1972**, *28*, 1229–1232. [[CrossRef](#)]
29. Mannervik, S. Optical studies of multiply excited states. *Physica Scr.* **1989**, *40*, 28–52. [[CrossRef](#)]
30. Madesis, I.; Laoutaris, A.; Zouros, T.J.M.; Benis, E.P.; Gao, J.W.; Dubois, A. Pauli Shielding and Breakdown of Spin Statistics in Multielectron Multi-Open-Shell Dynamical Atomic Systems. *Phys. Rev. Lett.* **2020**, *124*, 113401. [[CrossRef](#)]
31. Tanis, J.A.; Landers, A.L.; Pole, D.J.; Alnaser, A.S.; Hossain, S.; Kirchner, T. Evidence for Pauli Exchange Leading to Excited-State Enhancement in Electron Transfer. *Phys. Rev. Lett.* **2004**, *92*, 133201. [[CrossRef](#)]
32. Tanis, J.A.; Landers, A.L.; Pole, D.J.; Alnaser, A.S.; Hossain, S.; Kirchner, T. Erratum. *Phys. Rev. Lett.* **2006**, *96*, 019901. [[CrossRef](#)]
33. Zouros, T.J.M.; Sulik, B.; Gulyás, L.; Tökési, K. Selective enhancement of $1s2s2p^4P_J$ metastable states populated by cascades in single-electron transfer collisions of F⁷⁺($1s^2/1s2s^3S$) ions with He and H₂ targets. *Phys. Rev. A* **2008**, *77*, 050701. [[CrossRef](#)]
34. Strohschein, D.; Röhrbein, D.; Kirchner, T.; Fritzsche, S.; Baran, J.; Tanis, J.A. Nonstatistical enhancement of the $1s2s2p^4P$ state in electron transfer in 0.5–1.0-MeV/u C^{4,5+} + He and Ne collisions. *Phys. Rev. A* **2008**, *77*, 022706. [[CrossRef](#)]
35. Röhrbein, D.; Kirchner, T.; Fritzsche, S. Role of cascade and Auger effects in the enhanced population of the C³⁺($1s2s2p^4P$) states following single-electron capture in C⁴⁺($1s2s^3S$)-He collisions. *Phys. Rev. A* **2010**, *81*, 042701. [[CrossRef](#)]
36. Benis, E.P.; Zouros, T.J.M.; Gorczyca, T.W.; González, A.D.; Richard, P. Elastic resonant and nonresonant differential scattering of quasifree electrons from B⁴⁺(1s) and B³⁺($1s^2$) ions. *Phys. Rev. A* **2004**, *69*, 052718. [[CrossRef](#)]
37. Benis, E.P.; Zouros, T.J.M.; Gorczyca, T.W.; González, A.D.; Richard, P. Erratum. *Phys. Rev. A* **2006**, *73*, 029901. [[CrossRef](#)]

38. Curtis, L.J. A Diagrammatic Mnemonic for Calculation of Cascading Level Populations. *Am. J. Phys.* **1968**, *36*, 1123–1125. [[CrossRef](#)]
39. Cowan, R.D. *The Theory of Atomic Structure and Spectra*; University of California Press: Berkeley, CA, USA, 1981.
40. Shiina, Y.; Kinoshita, R.; Funada, S.; Matsuda, M.; Imai, M.; Kawatsura, K.; Sataka, M.; Sasa, K.; Tomita, S. Measurement of Auger electrons emitted through Coster–Kronig transitions under irradiation of fast C_2^+ ions. *Nucl. Instrum. Methods Phys. Res. Sect. B* **2019**, *460*, 30–33. [[CrossRef](#)]
41. Badnell, N.R.; Pindzola, M.S.; Griffin, D.C. Dielectronic recombination from the ground and excited states of C^{4+} and O^{6+} . *Phys. Rev. A* **1990**, *41*, 2422–2428. [[CrossRef](#)]
42. Stolterfoht, N. High resolution Auger spectroscopy in energetic ion atom collisions. *Phys. Rep.* **1987**, *146*, 315–424. [[CrossRef](#)]
43. Benis, E.P.; Zouros, T.J.M. Determination of the $1s2\ell 2\ell'$ state production ratios $^4P^0/{}^2P$, ${}^2D/{}^2P$ and ${}^2P_+/{}^2P_-$ from fast ($1s^2, 1s2s\ ^3S$) mixed-state He-like ion beams in collisions with H_2 targets. *J. Phys. B* **2016**, *49*, 235202. [[CrossRef](#)]
44. Mack, M.; Niehaus, A. Radiative and Auger decay channels in K-Shell excited Li-like ions ($Z = 6-8$). *Nucl. Instrum. Methods Phys. Res. Sect. B* **1987**, *23*, 109–115. [[CrossRef](#)]
45. Younger, S.M.; Wiese, W.L. Theoretical simulation of beam-foil decay curves for resonance transitions of heavy ions. *Phys. Rev. A* **1978**, *17*, 1944–1955. [[CrossRef](#)]
46. Zouros, T.J.M.; Lee, D.H. Zero Degree Auger Electron Spectroscopy of Projectile Ions. In *Accelerator-Based Atomic Physics: Techniques and Applications*; Shafrath, S.M., Austin, J.C., Eds.; AIP: Woodbury, NY, USA, 1997; pp. 426–479; Chapter 13.
47. Rigazio, M.; Kharchenko, V.; Dalgarno, A. X-ray emission spectra induced by hydrogenic ions in charge transfer collisions. *Phys. Rev. A* **2002**, *66*, 064701. [[CrossRef](#)]
48. Heckmann, P.H.; Träbert, E.; Bashkin, S.; *Introduction to the Spectroscopy of Atoms*; North-Holland: Amsterdam, The Netherlands, 1989.
49. Träbert, E. E1-forbidden transition rates in ions of astrophysical interest. *Physica Scr.* **2014**, *89*, 114003. [[CrossRef](#)]
50. Cheng, K.T.; Kim, Y.-K.; Desclaux, J.P. Electric dipole, quadrupole, and magnetic dipole transition probabilities of ions isoelectronic to the first-row atoms, Li through F. *At. Data Nucl. Data Tables* **1979**, *24*, 111–189. [[CrossRef](#)]
51. Chen, M.H. Dielectronic satellite spectra for He-like ions. *At. Data Nucl. Data Tables* **1986**, *34*, 301–356. [[CrossRef](#)]
52. Vainshtein, L.A.; Safronova, U.I. Dielectronic satellite spectra for highly charged H-like ions ($2l'3l'' - 1s2l, 2l'3l'' - 1s3l$) and He-like ions ($1s2l'3l'' - 1s^22l, 1s2l'3l'' - 1s^23l$) with $Z = 6 - 33$. *At. Data Nucl. Data Tables* **1980**, *25*, 311–385. [[CrossRef](#)]
53. Safronova, U.I.; Bruch, R. Transition and Auger Energies of Li-like ions ($1s2lnl'$ configurations). *Physica Scr.* **1994**, *50*, 45. [[CrossRef](#)]
54. Goryaev, F.F.; Vainshtein, L.A.; Urnov, A.M. Atomic data for doubly-excited states $2lnl'$ of He-like ions and $1s2lnl'$ of Li-like ions with $Z = 6 - 36$ and $n = 2, 3$. *At. Data Nucl. Data Tables* **2017**, *113*, 117–257. [[CrossRef](#)]
55. Davis, B.F.; Chung, K.T. Spin-induced autoionization and radiative transition rates for the $(1s2s2p)\ ^4P_J^o$ states in lithiumlike ions. *Phys. Rev. A* **1989**, *39*, 3942–3955. [[CrossRef](#)]
56. Benis, E.P.; Doukas, S.; Zouros, T.J.M.; Indelicato, P.; Parente, F.; Martins, C.; Santos, J.P.; Marques, J.P. Evaluation of the effective solid angle of a hemispherical deflector analyser with injection lens for metastable Auger projectile states. *Nucl. Instrum. Methods Phys. Res. Sect. B* **2015**, *365*, 457–461. [[CrossRef](#)]
57. Santos, J.P.; Parente, F.; Martins, M.C.; Indelicato, P.; Benis, E.P.; Zouros, T.J.M.; Marques, J.P. Radiative transition rates of $1s2s(^3S)3p$ levels for Li-like ions with $5 \leq Z \leq 10$. *Nucl. Instrum. Methods Phys. Res. Sect. B* **2017**, *408*, 100–102. [[CrossRef](#)]
58. Schneider, D.; Bruch, R.; Butscher, W.; Schwarz, W.H.E. Prompt and time-delayed electron decay-in-flight spectra of gas-excited carbon ions. *Phys. Rev. A* **1981**, *24*, 1223–1236. [[CrossRef](#)]
59. Mann, R. High-resolution K and L Auger electron spectra induced by single- and double-electron capture from H_2 , He, and Xe atoms to C^{4+} and C^{5+} ions at 10–100-keV energies. *Phys. Rev. A* **1987**, *35*, 4988–5004. [[CrossRef](#)] [[PubMed](#)]

60. Deveney, E.F.; Kessel, Q.C.; Fuller, R.J.; Reaves, M.P.; Bellantone, R.A.; Shafroth, S.M.; Jones, N. Projectile-Auger-electron spectra of C^{3+} following 12-MeV collisions with He targets. *Phys. Rev. A* **1993**, *48*, 2926–2933. [[CrossRef](#)] [[PubMed](#)]
61. Blanke, J.H.; Heckmann, P.H.; Träbert, E. Beam-Foil Lifetimes of Doubly-Excited $n = 3$ States of Three-Electron Ions C^{3+} - F^{6+} . *Physica Scr.* **1985**, *32*, 509. [[CrossRef](#)]
62. Blanke, J.H.; Heckmann, P.H.; Träbert, E.; Hucke, R. Quartet Term Systems of C^{3+} - F^{6+} Ions. *Physica Scr.* **1987**, *35*, 780–786. [[CrossRef](#)]
63. Laughlin, C. Calculations on transitions in singly- and doubly-excited C IV. *Zeitschrift Phys. D* **1988**, *9*, 273–277. [[CrossRef](#)]
64. Kramida, A. Corrigendum to “Configuration interactions of class 11: An error in Cowan’s atomic structure theory” [Comput. Phys. Commun. 215 (2017) 47–48]. *Comput. Phys. Commun.* **2018**, *232*, 266–267. [[CrossRef](#)]
65. Sisourat, N.; Pilskog, I.; Dubois, A. Non perturbative treatment of multielectron processes in ion-molecule scattering: Application to He^{2+} - H_2 collisions. *Phys. Rev. A* **2011**, *84*, 052722. [[CrossRef](#)]
66. Gao, J.W.; Wu, Y.; Wang, J.G.; Sisourat, N.; Dubois, A. State-selective electron transfer in He^+ +He collisions at intermediate energies. *Phys. Rev. A* **2018**, *97*, 052709. [[CrossRef](#)]
67. Sisourat, N.; Dubois, A. Semiclassical close-coupling approaches. In *Ion-Atom Collision—The Few-Body Problem in Dynamic Systems*; Schultz, M., Ed.; de Gruyter: Berlin, Germany; Boston, MA, USA, 2019; pp. 157–178.
68. Madesis, I.; Laoutaris, A.; Zouros, T.J.M.; Nanos, S.; Benis, E.P. Projectile electron spectroscopy and new answers to old questions: Latest results at the new atomic physics beamline in Demokritos, Athens. In *State-of-the-Art Reviews on Energetic Ion-Atom and Ion-Molecule Collisions*; Interdisciplinary Research on Particle Collisions and Quantitative Spectroscopy; Belkić, D., Bray, I., Kadyrov, A., Eds.; World Scientific: Singapore, 2019; Volume 2, pp. 1–31, Chapter 1.



© 2020 by the authors. Licensee MDPI, Basel, Switzerland. This article is an open access article distributed under the terms and conditions of the Creative Commons Attribution (CC BY) license (<http://creativecommons.org/licenses/by/4.0/>).